ROMANIAN JOURNAL OF INFORMATION SCIENCE AND TECHNOLOGY
Volume **18**, Number 4, 2015, 343–355

Detection of Magnetic Nanoparticles for Lab-on-a Chip Applications

Marius VOLMER[1], Marioara AVRAM[2], Andrei Marius AVRAM[2]

[1] Transilvania University of Brasov, Eroilor 29, Brasov 500036, Romania
E-mail: volmerm@unitbv.ro

[2] National Institute for Research and Development in Microtechnologies, 32B Erou Iancu Nicolae Str., 72996 Bucharest, Romania
E-mail: marioara.avram@imt.ro

Abstract. Detection of magnetic carriers used as labels for biosensing applications represent key features in lab-on-a-chip (LOC) devices. This paper presents a review of some experimental techniques used by us to characterize magnetic nanoparticles and to detect them using Permalloy based planar Hall effect sensors. We found that sensitivities better than $0.2x10^{-3}$ emu/mV can be obtained for specific detection schemes. A freeware micromagnetic simulator, SimulMag, was used to complete the view on these experiments.

Keywords: Magnetic nanoparticles; Planar Hall effect sensors; Micromagnetic simulations; Lab-on-chip.

1. Introduction

The superparamagnetic (SPM) micro- nanoparticles are widely used to tag, manipulate, and detect chemical and biological species. This functionality is exploiting in what is known as lab-on-a-chip devices (LOC). The idea of lab-on-a-chip is basically to reduce the size and the price of biological or chemical laboratories. Another advantage is that lab-on-a-chip requires very small amounts of reagents/chemicals.

Lab-on-a-chip systems can be made out of silicon, glass and polymeric materials. The typical microfluidic channel dimensions are in the range of several tens to hundreds of μm. Liquid samples or reagents can be transported through the microchannels from reservoirs to reactors using electrokinetic, magnetic, or hydrodynamic pumping methods. As a new concept, it has been shown that strong, localized

stray fields from domain walls (DWs) in micrometre ferromagnetic tracks can trap individual SPM particles with forces up to hundreds of pN and manipulate them [1]. Fluidic motions or biochemical reactions can be monitored using various sensors.

Detection of the fields generated by magnetic nanoparticles (MNPs) which are used to label chemical or biological species of interest can be made using giant magnetoresistive (GMR), magnetic tunnel junctions (MTJ) or planar Hall effect (PHE) sensors [2–6]. The sensor used in this study is based on PHE, schematically illustrated in Fig. 1.

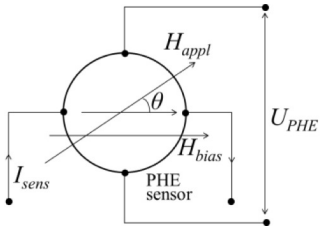

Fig. 1. Schematic illustration of the PHE sensor.

The PHE is due to the anisotropic magnetoresistance (AMR) effect found in magnetic materials. A study presented in [7] clearly illustrates the field dependence of the AMR effect using a typical Hall effect measurement setup which is, from electrical point of view, similar to a Wheatstone bridge. In such experiments the field is applied in the film plane, like in Fig. 1. It was found a quadratic dependence of the PHE signal on the magnetization, M, in Ni, Co, Fe, and Ni_xFe_{1-x} films. The output signal also shows an angular dependence such that a general equation, of the type $U_{PHE} \sim I_{sens} \cdot M^2 \cdot \sin 2\theta$, can be used to describe the PHE signal; θ is the angle between the magnetization vector and the driving current through the sensor, I_{sens}. In turn, M depends on the applied field and the signal can be used as a probe of the structure magnetization.

Structures like NiFe(5 nm)/IrMn(20 nm)/NiFe(20 nm) [8] or exchange biased spin valves like NiFe(16 nm)/Cu(1.2 nm)/NiFe(2 nm)/IrMn(15 nm) [5, 9] are among the most used to deposit cross-shaped PHE sensors (NiFe - Permalloy). Because of the exchange interaction, H_E, between the antiferromagnetic layer (IrMn) and the ferromagnetic layer (NiFe), an ordered magnetization state can be found in the absence of a biasing field. Also, the anisotropy field, H_K, which can be defined during the deposition process, may favour the establishment of magnetization in the sensing layer over a particular direction. However it has to mention that the field sensitivity of the PHE signal, S, depends on H_E and H_K as $S \sim 1/(H_E + H_K)$. Higher values of H_K and H_E can assure a well ordered magnetic state in the sensing layer but lower the field sensitivity of the PHE signal. Therefore, a compromise must be found depending on the application we are following. Sensitivities between 3 μV/Oe to 7 μV/Oe for a driving current of 1 mA trough the sensor are reported for applied fields in the range of ±15 Oe [4-6, 8, 9]. It should be noted that other geometries like ring-shape [10] or elliptical-shape structures have been considered to increase, by a geometrical factor, the PHE signal. However, by this study, we demonstrate that very good results can

be obtained by using disk shaped PHE sensors made from Permalloy. Depending on the biasing field, we found sensitivities up to 6 μV/(Oe·mA).

The MNPs polarizedby a dc or ac magnetic field can affect the magnetization state of the PHE sensor,leading to a detectable signal. It is to mention that results from theoretical modelling, as well as laboratory tests, show that micrometre sized spin-valve sensors can resolve single magnetic nanoparticles [4, 8, 9]. The external magnetic field can be applied either parallel or perpendicular to the sensor surface. Because the value of the demagnetising field over a direction perpendicular to the film surface is so large, the spin-valve devices are mostly sensitive for in plane magnetic fields. Therefore, it is possible to apply a rather large magnetizing field in the out-of-plane orientation of the magnetoresistive sensor without directly affecting the sensor itself [11, 12].

A freeware micromagnetic simulator, SimulMag [13], was used to analyse the system composed of sensor and magnetic nanoparticles in order to explain some experimental results.

2. Results and discussion

2.1. Characterization of planar Hall effect sensors

Using typical photolithographic technique, Permalloy based PHE sensors, 1 mm diameter and 20 nm thick, were patterned on to oxidized Si substrate. No anisotropy axis has been induced during the deposition process. Four PHE sensors were defined and interconnected on a chip, Fig. 2a. To control the sensor sensitivity and linearity, a biasing field has been applied along the driving current, Fig. 2. By this, different magnetization states in the sensor layer can be generated.

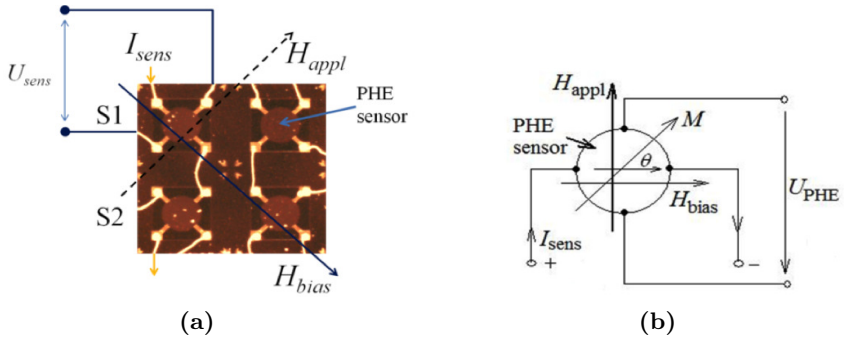

(a) **(b)**

Fig. 2. (a) Top view of the chip with 4 PHE sensors and (b) the schematic used to explain the characterization setup. The biasing field, H_{bias}, and the applied field, H_{appl}, directions are illustrated. The electrical connections are indicated.

A 200 nm thick TiO_2 layer was sputtered on the sensor surface to protect against the fluid used during the experiments. The chip with PHE sensors was placed inside a

system composed of Helmholtz coils which are able to generate well defined and uniform magnetic fields over three orthogonal directions; two of these fields were applied in the film plane. The measurement system, used to study the field dependencies of the AMR and PHE effects, consists in Keithley 6221 programmable current source, Keithley 2182A nanovoltmeter, and three programmable high current sources. The DC driving current through the sensors, I_{sens} = 5 mA, was chosen to maximize the output signal but without affecting the thermal stability of the structure. The resistance between the current or between the voltage contacts is about 120 Ω, Fig. 2a. A DC detection setup was used to read out the sensor because the frequency of the sweeping magnetic field was 0.01 Hz. The integration time, i.e. the period of time the input signal is measured, was 20 ms. A digital filter has been used. For each displayed reading, five measurements were averaged. This offers the best compromise between noise performance and speed. For this setting, the noise level was about 35 nV peak-to-peak.

The low field dependencies of the PHE signal, measured for the sensor S1, are presented in Fig. 3a. The applied field is in the film plane, perpendicular to the driving current, I_{sens}, as is illustrated in Fig. 2a. Voltage offsets have been subtracted. In Fig. 3b is ploted the field sensitivity, S, as a function of the biasing field.

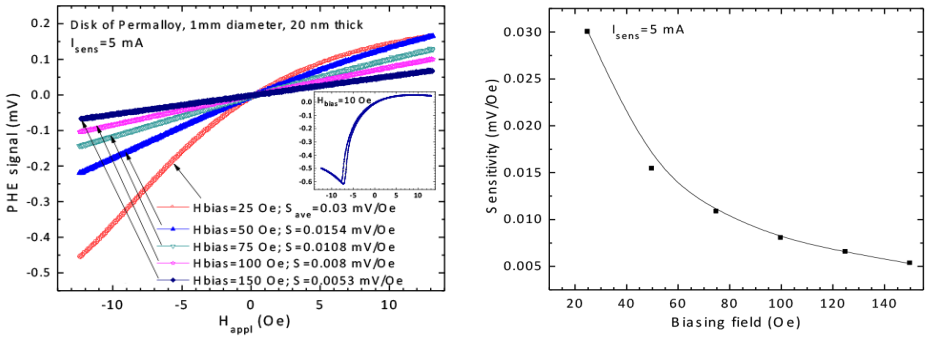

(a) **(b)**

Fig. 3. (a) The low field dependencies of the PHE signal for different biasing fields and (b) the dependence of the field sensitivity on the biasing field, H_{bias}. The inset in Fig. 3a shows the field dependence of the PHE signal for H_{bias}=10 Oe; the nonlinear behaviour is evidenced.

For biasing fields smaller than 25 Oe the field dependencies $U_{PHE}(H_{appl})$ show a nonlinear behaviour and hysteretic effects. This is because the magnetization processes are more complex, presenting magnetic moments rotation and domain walls movement which generates nonlinearity and hysteretic effects. The very good linearity of the measured signal for H_{bias} higher than 25 Oe shows that the main mechanism of the magnetization reversal processes that take place in the sensing layer is based on the magnetic moments rotation. The output voltage is mainly proportional with $\sin 2\theta$ which presents linear field dependence for small values of H_{appl}. However, as for high values of H_E and H_K, higher torque is needed to rotate the magnetic moments

and the field sensitivity decreases as is illustrated in Fig. 3. Therefore, depending on the desired application and the measurement range, the adequate biasing field can be chosen.

2.2. Magnetic characterization of maghemite nanoparticles

The magnetite or maghemite nanoparticles, which are among the most used for LOC applications, show superparamagnetic (SPM) behaviour above the blocking temperature, T_B, *i.e.*, the measured magnetic moment in the absence of an external magnetic field is zero. This SPM behaviour is useful in LOC applications because can be avoided unwanted capture of the MNPs over the sensors surface and can be minimised false detection signals when magnetic sensors are used.

The magnetization curves for maghemite nanoparticles and for functionalized maghemite nanoparticles with Polyethylene glycol (PEG) 6000 were measured by using the VSM unit from 7T Mini Cryogen Free Measurement System from Cryogenic.

A well-established method to determine the blocking temperature is to perform Zero Field Cooling-Field Cooling (ZFC-FC) magnetization measurements. From the ZFC-FC measurements, Fig. 4a, made on maghemite nanoparticles, 10 nm in diameter, we have obtained $T_B = 252$ K. The room temperature magnetization curve for these MNPs shows a typical SPM behaviour, Fig. 4b.

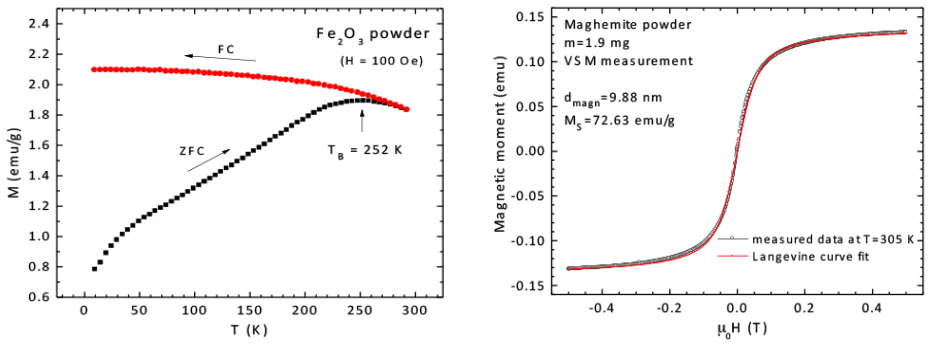

(a) **(b)**

Fig. 4. (a) The ZFC-FC magnetization curves and (b) the magnetization curves obtained by VSM for maghemite nanoparticles; the particle diameter is determined from the curve fitting.

The magnetization curve is well fitted by the Langevin function (1) indicating the superparamagnetism of the nanoparticles [2]:

$$M(H) \approx M_S \left(1/\tanh(\alpha) - 1/\alpha\right), \quad \alpha = \frac{\mu_0 H \cdot m_S}{K_B T} \tag{1}$$

where $m_s = \pi d^3 M_S/6$ and $M_S = 480$ emu/cm^3=480 kA/m (for maghemite).

From the fitting curve we found an average value of the particle diameter, $d_{magn} =$ $= 9.88$ nm, which is consistent with the XRD measurements made on the same type of powder.

The magnetization curves for maghemite nanoparticles functionalized with Polyethylene glycol (PEG) 6000 were measured at room temperature and presented in Fig. 5 and Fig. 6. Figure 5a shows the magnetization curve obtained by VSM at room temperature for 30 µl of aqueous solution containing maghemite nanoparticles functionalized with PEG 6000. The magnetization curve is strongly affected at higher fields by the diamagnetic behaviour due to water and PEG molecules. Figure 5b presents the magnetization curves for the same solution when diamagnetic correction is applied.

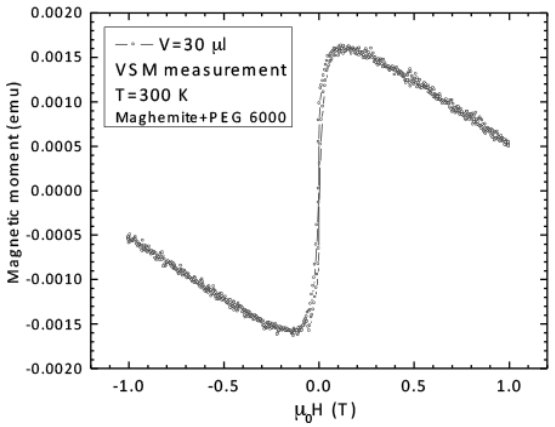

(a)

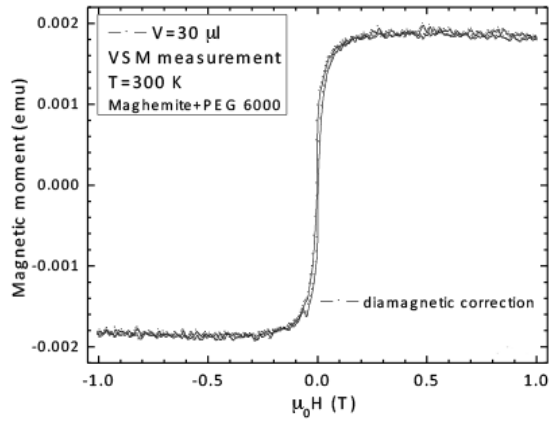

(b)

Fig. 5. (a) The magnetization curve obtained by VSM at room temperature for 30 µl of aqueous solution containing maghemite nanoparticles functionalized with PEG 6000 and (b) the same curve when diamagnetic correction is applied.

Figure 6a presents the high field magnetization curve, as measured, for 1.27 mg powder of functionalized maghemite nanoparticles. The high field magnetization curve, allows us to estimate the diamagnetic contribution of the PEG 6000 molecules. To obtain 1.27 mg of powder, we used 107.7 mg of aqueous solution which was dried at 56℃. We used this approach in order to lower the diamagnetic contribution, due to water molecule, and to obtain the "magnetic diameter" of the functionalized maghemite nanoparticles. After applying the diamagnetic correction and fitting the magnetization data from Fig. 6b with the Langevin function, we obtained $d_{magn} = 11.48$ nm.

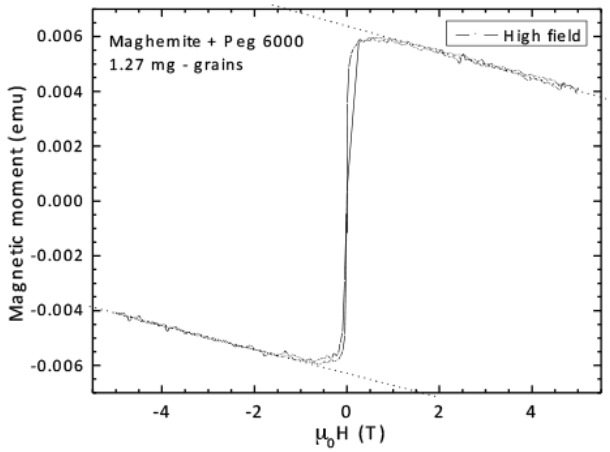

(a)

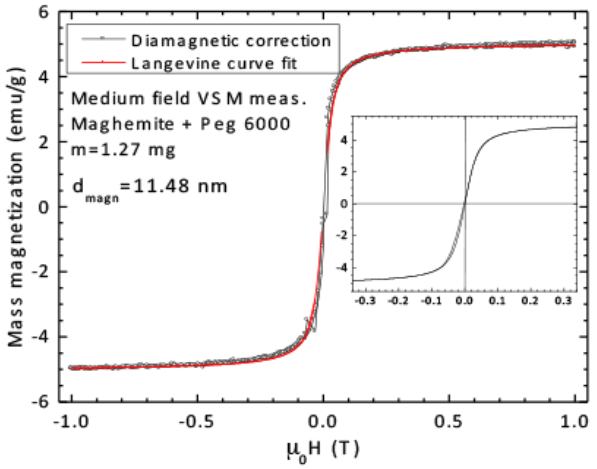

(b)

Fig. 6. (a) Magnetization curve obtained by VSM for maghemite nanoparticles functionalized with PEG 6000 as powder and (b) the extracted curve after diamagnetic correction; the inset shows the low field magnetization curve.

2.3. Detection of magnetic nanoparticles by Planar Hall Effect sensors

From Fig. 6 it comes that MNPs have to be magnetized in fields higher than 100 Oe (*i.e.*, 0.01 T in air) to reach a large enough magnetization state that can be detected by the PHE sensor. On the other hand, the PHE sensors saturate for $H_{appl} > 25$ Oe. Therefore, in order to avoid the sensor saturation, we chose to apply the magnetizing field, H_{appl}, perpendicular to the sensor surface. Because the sensor is less sensitive to perpendicular fields no higher than hundreds of Oe, only the in plane components of the field generated by MNPs will produce significant changes of the magnetization in the sensing layer.

For detection experiments we placed one drop of 0.7 μl of aqueous solution with functionalized maghemite nanoparticles on the sensor surface. Evaporation of water was carried out in a magnetic field ($H_{appl} = 130$ Oe) applied perpendicular to the sensor surface previously polarized closed to the coercive state. The current through the sensor was $I_{sens} = 5$ mA. In these conditions the MNPs have been retained inside of the sensor surface because of the complex domain structure, typical for a coercive state, which generates stray fields perpendicular to the surface. We showed this behaviour by micromagnetic simulations [14]. For a uniform magnetized state of the sensor layer, the MNPs will accumulate near edges where normal components of magnetization can be found [15].

The detection scheme was as follows: the applied field, perpendicular to the sensor surface, was swept between ±140 Oe while H_{bias} was kept constant at different values. Measurements were made without and with MNPs on the sensor surface. The results are presented in Fig. 7 for $H_{bias} = 0$, ±8 Oe and ±16 Oe respectively. Two cycles have been scanned for each measurement to see data repeatability. These plots have the same shape like the field dependencies of the PHE signal, for low biasing fields, plotted in Fig. 3a. The sign of the slopes depends on the polarity of the sensor magnetization through the biasing field.

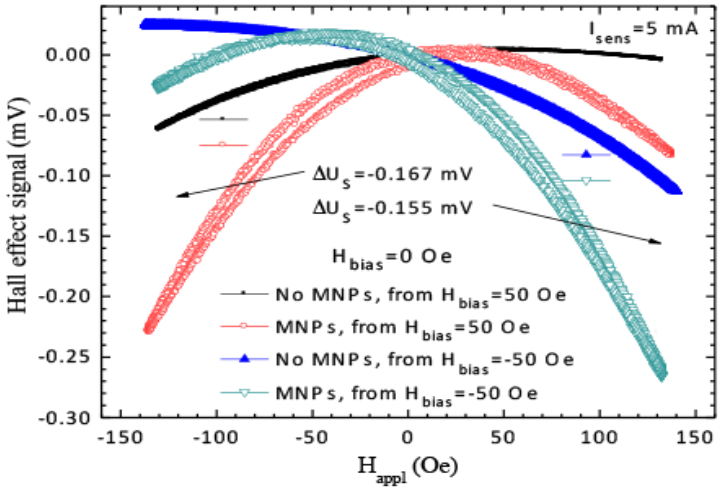

Fig. 7a.

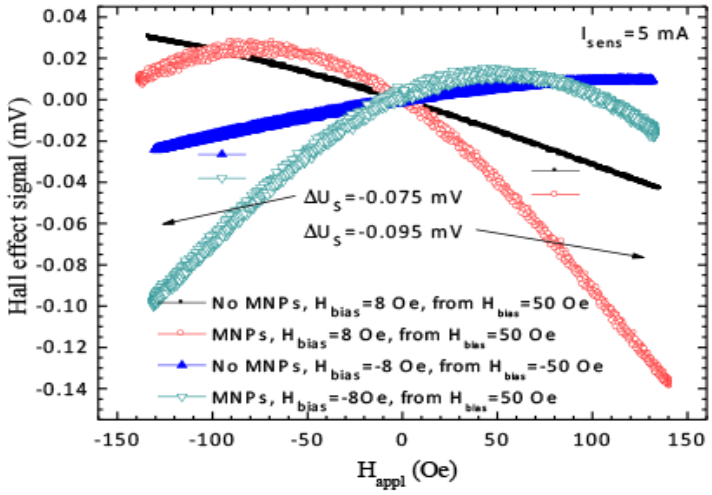

Fig. 7b.

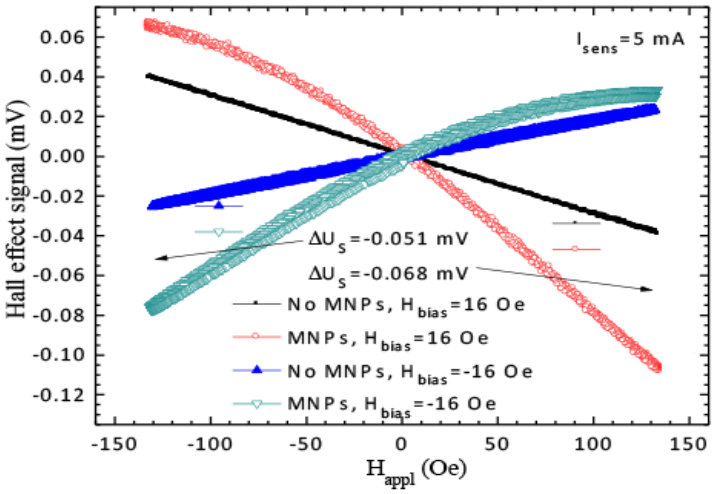

Fig. 7c.

Fig. 7. The field dependencies of the sensor signal when H_{appl} is swept between ±140 Oe for (a) $H_{bias} = 0$, (b) $H_{bias} = \pm 8$ Oe and (c) $H_{bias} = \pm 16$ Oe respectively.

The presence of MNPs over the sensor surface will generate in-plane components of the magnetic field which is responsible for the appearance of the PHE signal. Even in the absence of MNPs, a small in-plane magnetic field is found in the sensor layer because (i) of small misalignment of the applied field from the perpendicular direction and (ii) because of the nature of the sensing layer that bends the field lines. To illustrate this behaviour, we present in Fig. 8 the results of micromagnetic simulations made on disc shaped structure of Permalloy, 2 μm in diameter and 20 nm

thick for $H_{bias} = 10$ Oe and H_{appl} perpendicular to the surface. Details regarding the structure design and micromagnetic setup used for simulations can be found in [11, 12]. The results give a good qualitative agreement with data presented in Fig. 7a,b and explain the shape of the experimental dependencies obtained for the PHE signal when H_{appl} is directed perpendicular to the sensor surface.

When $H_{bias} = 0$, the sensor is in remnant state which depends on the initial magnetization as shown in Fig. 7a where are plotted the field dependencies of the PHE signal for states that originate from $H_{bias} = 50$ Oe and –50 Oe respectively. The large variation of the PHE signal and the hysteretic effects are in good agreement with data presented in Fig. 3a for low biasing fields. The remnant steady state can be easily affected by small electromagnetic perturbations because Permalloy is a soft magnetic material. By this, the sensor response will change. To have data repeatability, the sensor has to be re-polarized by applying a pulse of +50 Oe or –50 Oe before making the measurements for $H_{bias} = 0$. When the biasing field increases, the signal linearity increases but the field sensitivity decreases, as it was presented also in Fig. 3. The field dependencies of PHE signal for $H_{bias} = \pm 8$ Oe and $H_{bias} = \pm 16$ Oe are presented in Fig. 7b and Fig. 7c respectively. The modulus of the signal amplitude decreases from about 0.085 mV, Fig. 7b, to 0.06 mV, Fig. 7c. As is expected, the maximum difference between the signal with MNPs and without MNPs appears for the maximum value of the applied field, ±140 Oe, where the particles acquire a larger magnetic moment.

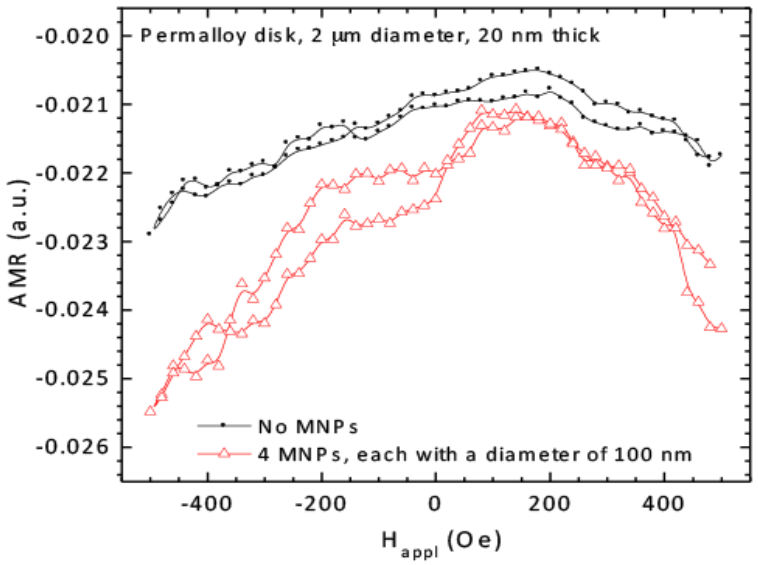

Fig. 8. Results of the micromagnetic simulations of the sensor output without MNPs and with 4 MNPs of maghemite, 100 nm diameter, placed over the sensor surface; H_{appl} is perpendicular to the sensor surface.

To estimate de amount of the magnetic moment detected by the sensor and hence the corresponding mass of the maghemite NPs functionalized with PEG 6000, we used

data from Fig. 5 and Fig. 6. The magnetic moment for 0.7 μl aqueous solution at 140 Oe (0.014 T) is about 2.33×10^{-5} emu. After water evaporation, this magnetic moment produces a variation between –0.16 mV to –0.06 mV of the output signal, Fig. 7. This means sensitivities between 1.456×10^{-4} emu/mV to 3.88×10^{-4} emu/mV. So, magnetic moments of the order of 10^{-6} emu can be easily detected.

By using data from Fig. 6b we get a value of 9.71 μg powder composed from maghemite functionalized with PEG 6000. It should be noted that for this value of the applied field the diamagnetic contribution can be neglected. This means about 1.26 μg of pure maghemite cores. The estimation was obtained by using the above results and by comparing the magnetization curves for pure maghemite powder, Fig. 5b and functionalized maghemite with PEG 6000, Fig. 6b.

Finally, we present an interesting behaviour when the sensor is polarized between the remnant and the coercive states. Small in plane perturbations due to the applied field and MNPs can lead the sensor very close to the coercive state. The coercive field is about ±8 Oe. We present, in Fig. 9, the field dependencies of the sensor signal when H_{appl} is swept between ±150 Oe for (a) $H_{bias} = 4$ Oe and (b) $H_{bias} = -4$ Oe. The state for $H_{bias} = 4$ Oe is obtained by coming from $H_{bias} = -40$ Oe to 0 and then to 4 Oe. The state for $H_{bias} = -4$ Oe is obtained by coming from $H_{bias} = 40$ Oe to 0 and finally to –4 Oe.

This behaviour of the sensor magnetization is reflected by the field dependence of the PHE signal. We see how the starting and ending points, for two complete cycles, are in different positions. Such values of the biasing fields, close to the coercive field, can generate large signal variation but as a singular pulse which is not repeating in amplitude for the next field cycles. The structure has to be re-magnetised like described above. The presence of MNPs over the sensor surface increases the amplitude of PHE signal variation and the distance between initial and final state. This technique can be used for high sensitivity MNPs detection.

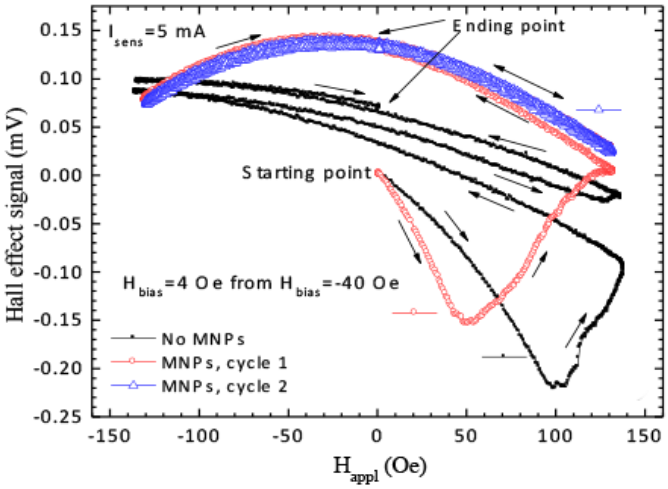

Fig. 9a.

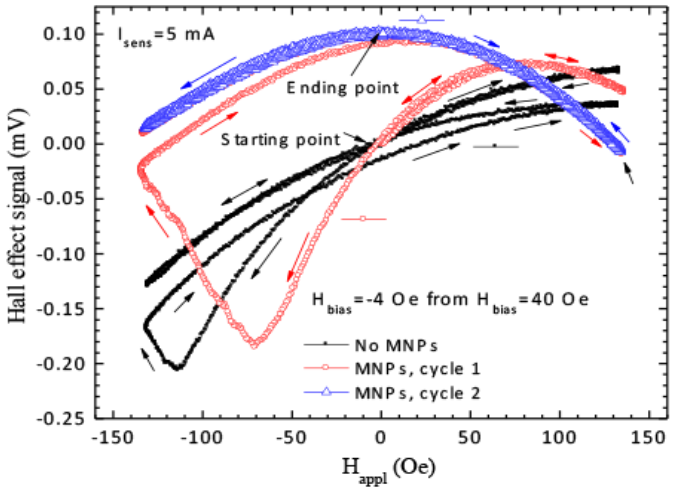

Fig. 9b.

Fig. 9. The field dependencies of the sensor signal when H_{appl} is swept between ±150 Oe for (a) H_{bias} = 4 Oe and (b) H_{bias} = –4 Oe; initially the sensor was polarised at H_{bias} = –40 Oe, Fig. 9a and H_{bias} = 40 Oe, Fig. 9b. The arrows are guides for the eyes.

3. Conclusions

Aspects regarding characterization of PHE sensors, magnetic properties of maghemite based nanoparticles used for LOC applications and detection of these MNPs with PHE sensors have been presented in this study. A home-made characterization system, composed from Helmholtz coils and special electrical setup, has been developed in order to control with precision the sensor magnetization state and to perform the characterization and detection experiments.

We found high detection sensitivities, up $1.456x10^{-4}$ emu/mV, for different magnetization states in the sensing layer, which means that magnetic moments of the order of 10^{-6} emu can be detected with the setup described. We observed large signal variations of the sensor output when the magnetic layer is polarized close to the coercive state. So, particular magnetization states, like remnant or coercive, can provide convenient methods for the capture and detection of MNPs.

Further experiments which employ the using of special combinations of DC and AC magnetic fields will be made. The main limitation of our system, in what concerns the lowest magnetic moment that can be detected, comes from the relatively large dimension of the PHE sensors. Spintronic structures will be considered to develop such type of microsensors and the chip will be integrated in a microfluidic system. By lowering the sensor's dimension to micrometre scale and integrating the biasing system in the same chip, a better control of the magnetization state in the sensing layer will be possible and higher detection sensitivities can be obtained.

Acknowledgments. The authors are grateful for the financial support from the project PN2 CELLIMUNOCHIP No. 2/2012 in the frame of the National Partnership program.

References

[1] RAPOPORT E., MONTANA D., BEACH G. S. D., Lab Chip **12**, pp. 4433–4440 (2012).

[2] LI G., SUN S., WILSON R. J., WHITE R. L., POURMANDC N., WANG S. X., Sensors Actuators A **126**, pp. 98–106 (2006).

[3] GERMANO J., MARTINS V. C., CARDOSO F. A., ALMEIDA T. M., SOUSA L., FREITAS P. P., PIEDADE M. S., Sensors **9**(6), pp. 4119–4137, (2009).

[4] CHUI K. M., ADEYEYE A. O., MO-HUANG LI, J. Magn. Magn. Mater. **310**, e992-e993 (2007).

[5] TU B. D., CUONG L. V., HUNG T. Q., HUONG GIANG D. T., DANH T. M., DUC N. H., KIM C., IEEE Trans. Magn. **45**(6), pp. 2378–2382 (2009).

[6] DAMSGAARD C. D., FREITAS S. C., FREITAS P. P., HANSEN M. F., J. Appl. Phys. **103**, 07A302 (2008).

[7] PRADOS C., GARCIA D., LESMES F., FREIJO J. J., HERNANDO A., Appl. Phys. Lett. **67**(5), pp. 718–720 (1995).

[8] EJSING L., HANSEN M. F., MENON A. K., FERREIRA H. A., GRAHAM D. L., FREITAS P. P., J. Magn. Magn. Mater. **293**, pp. 677–684 (2005).

[9] TRAN QUANG HUNG, SUNJONG OH, JONG-RYUL JEONG, CHEOLGI KIM, Sens. Actuators A **157 (**1), pp. 42–46 (2010).

[10] SINHA B., OH S., RAMULU T. S., LIM J., KIM D. Y., KIM C., Advanced Materials Research **317–319**, pp. 1136–1140 (2011).

[11] VOLMER M., AVRAM M., J. Nanosci. Nanotechnol. **12**, pp. 7456–7459 (2012).

[12] VOLMER M., AVRAM M., Microelectron. Eng., **108**, pp. 116–120 (2013).

[13] PC Micromagnetic Simulator, `http://math.nist.gov/oommf/contrib/simulmag/`

[14] VOLMER M., AVRAM M., AVRAM A. M., IEEE 38th International Semiconductor Conference, CAS 2015; Sinaia; Romania, 12–14 Oct. 2015, pag. 117–120, ISBN 978-1-4799-8862-4; DOI: 10.1109/SMICND.2015.7355180.

[15] ØSTERBERG F. W., DALSLET B. T., DAMSGAARD C. D., FREITAS S. C., FREITAS P., HANSEN M. F., IEEE Sensors J. **9**, pp. 682–688 (2009).